User Mobility Analysis in Disjoint-Clustered Cooperative Wireless Networks

Wei Bao, Yonghui Li, and Branka Vucetic
Faculty of Engineering and Information Technologies, University of Sydney
{wei.bao,yonghui.li,branka.vucetic}@sydney.edu.au

ABSTRACT

Base station (BS) cooperation has been regarded as an effective solution to improve network coverage and throughput in next-generation wireless systems. However, it also introduces more complicated handoff patterns, which may potentially degrade user performance. In this work, we aim to theoretically quantify users' handoff performance in disjoint-clustered cooperative wireless networks. It is a challenging task due to spatial randomness of network topologies. We propose a stochastic geometric model on user mobility, and use it to derive a theoretical expression for the handoff rate experienced by an active user with arbitrary movement trajectory. As a study on the application of the handoff rate analysis, we furthermore characterize the average downlink user data rate under a common non-coherent joint-transmission scheme, which is then used to derive a tradeoff between handoff and data rates in a network with an optimal cooperative cluster size. Finally, extensive simulations are conducted to validate our analysis.

1 INTRODUCTION

Base station (BS) cooperation has been shown to be an effective approach to improve the performance of cellular networks. Compared with the traditional single-BS association, BS cooperation can significantly enhance the received power levels of users and thus they are less likely to enter a dead spot, where the received signal-to-interference-plus-noise ratio (SINR) becomes too low.

The implementation of BS cooperation can be classified into two broad categories: disjoint cluster and user-centric cluster. In the disjoint cluster mode, the entire BS set is partitioned into multiple non-overlapping subsets, and the BSs in each subset cooperatively serve users within their service range. In the user-centric cluster mode, each user is served by its individually selected set of neighboring BSs. Disjoint cluster is easier to implement compared with user-centric cluster. In the user-centric mode, user-dependent cooperative BS clusters are inevitably overlapped, so that all BSs and users are coupled with each other, leading to complex resource allocation and user scheduling problems, as well as potentially heavy signalling overhead. In contrast, in the disjoint cluster mode, BS clusters are non-overlapped, and users in one BS cluster are served by the same set of BSs. Different clusters could operate independently so that it is more straightforward to coordinate them.

In this paper, we focus on the mobility management in disjoint-clustered cooperative networks. However, the patterns of network topology are substantially different compared with those in traditional single-BS association systems, since the handoffs involve changes in sets of multiple BSs. We need to characterize the region of a BS cluster (i.e., the region where a user connects with the same BS set). If a user crosses the boundary between two clusters, its connection BS set is changed and a handoff is made. However, due to the spatial irregularity of BSs (caused by emerging technologies such as plug-and-play BSs and ultra-dense BSs) as well as disjoint-clustered BS cooperation, the cluster boundaries are generated randomly and irregularly. Fig. 1(a) shows the cell splitting if users are served by one closest BS, while Fig. 1(b) shows the scenario where users are served by a cluster of BSs. Previously developed techniques for single-BS handoff analysis [9, 10, 19, 24, 31] are insufficient to model the complex handoff patterns in such cooperative wireless networks.

Characterizing the handoff rate provides important guidelines for system design. One main design concern is the tradeoff between the handoff rate and the data rate. In this paper, we focus on optimizing the cluster size, by taking both the handoff cost and the data rate into consideration.[1]

For the analysis we introduce a new stochastic geometric theoretical framework to quantify the handoff rate in a disjoint-clustered cooperative wireless network. We model the BS location distribution as a Poisson point process (PPP) to capture their spatial randomness. Our contributions are as follows:

- Through stochastic and analytic geometric analysis, we derive an exact expression for the handoff rate experienced by an active user with arbitrary movement trajectory.
- We calculate the average downlink data rate of users under the non-coherent joint-transmission (NC-JT) scheme [27, 35].
- We characterize the optimal cluster size, to calculate the tradeoff between handoff rate and data rate. Then, we derive an approximated optimal cluster size in a simple closed form, which is shown to be accurate under a variety of parameter settings.

The rest of this paper is organized as follows. In Section 2, we discuss the relation between our approach and prior results. In Section 3, we describe the system model. In Section 4, we present the theoretical analysis on the handoff rate in the system. In Section 5, we consider the optimal cluster size by accounting for the impacts of both the handoff cost and the data rate. In Section 6, we validate our analysis with simulation. Finally, conclusions are given in Section 7.

2 RELATED WORK

2.1 Stochastic Geometric Analysis

Stochastic geometry is an effective mathematical modeling tool to analyze the performance of wireless networks with random spatial distributions of users and BSs. In the single-BS association scenario,

[1]Note that the optimal cluster size remains an open problem, as there are diverse factors to be considered, such as data rate, handoff rate, communication overhead, and computational complexity in signal processing. The exact characterizations of factors other than the handoff rate and data rate are out of the scope of this paper.

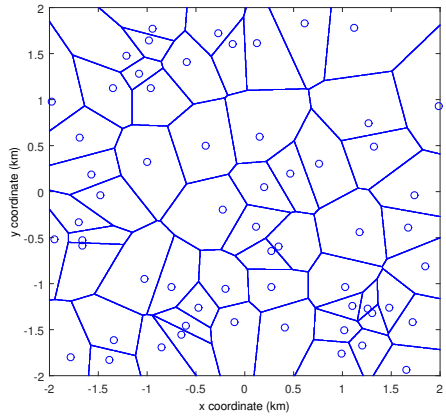

(a) Single-BS association case. The set of blue lines shows cell boundary.

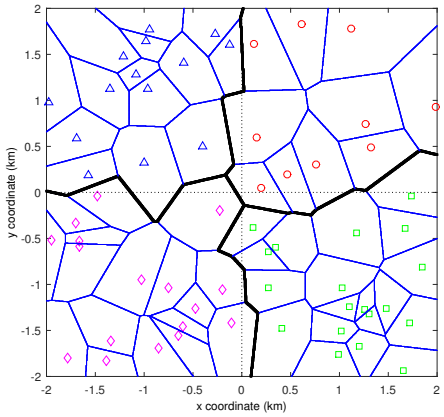

(b) Disjoint-clustered BS cooperation. BSs are grouped into four clusters in the four squares separated by the dotted lines. The set of thick black lines shows cluster boundary.

Figure 1: A comparison of single-BS association and disjoint cluster.

performance metrics such as interference distribution, coverage probability, data rate, and throughput are analyzed in multiple publications such as [13, 14, 21, 33].

In cooperative networks, a two-BS cooperation model was proposed and the user coverage probability was derived for this model [7]. In [2, 17, 20], various forms of the disjoint cluster mode of BS cooperation were considered. In [22, 23, 27, 28, 35, 37], the performance of different joint transmission schemes in user-centric BS cooperation was evaluated, such as NC-JT [27, 35], synchronous joint transmission [28], interference nulling [23], and coordinated beamforming [22, 37]. All of these papers focused only on networks with stationary users, and thus handoffs were not considered.

2.2 Handoff Analysis in Wireless Networks

Most existing handoff analysis is concerned only with the single-BS association scenario. One well-known category of analysis techniques employs queueing formulation, without explicitly modeling the geometric patterns of cell shapes in the networks [4, 8, 12, 15]. In these approaches, cells were modeled as queues containing active users, and handoffs were modeled as unit transfers between queues. Another common category of analysis techniques assume regularly gridded cells for mathematical convenience. Examples of such geometric topologies include hexagonal grids [3, 29], square grids [32], and circles overlaying hexagons [18].

To further capture the spatial randomness of network topologies, a seminal study on user mobility was conducted in [24] for a single-tier cellular network with randomly distributed BSs, where the BSs were modeled as a homogeneous PPP, and cell splitting was modeled as a standard Poisson Voronoi. The case of multi-tier cellular networks was considered in [10, 30, 31], where each tier of BSs was modeled as a homogeneous PPP, and the resultant cell splitting was modeled as a weighted Poisson Voronoi. Further extension to [10] was given in [9], where the BS tiers were modeled as Poisson cluster processes (PCPs), such that their aggregation around highly populated areas could be accommodated. However, the above papers considered only single-BS association, which is not applicable to BS cooperative wireless networks.

The work most relevant to this paper is [11]. It characterized user mobility in cooperative wireless networks using stochastic geometric analysis. However, [11] considered the user-centric scenario, so that the analyses of both handoff rate and data rate are different from those in the disjoint-clustered scenario considered in this paper. Besides the challenge of accommodating the random network topology, we manage to address two additional challenges in the disjoint-clustered scenario: (1) Users are not always in the center of a cluster so that we need to consider the distribution of the relative user coordinates with respect to the cluster center; and (2) the expressions of handoff rate and data rate are not in closed form but with levels of integrations (which is inevitable due to the stochastic geometric analysis).

3 SYSTEM MODEL

We consider a cellular network with spatially randomly distributed BSs. In order to characterize their random spatial patterns, we employ the conventional assumption that the BSs form a homogeneous Poisson point process (PPP) [2, 7, 13, 14, 17, 20–23, 27, 28, 33, 35, 37] in two-dimensional Euclidean space $\mathbb{R}^2$. Let Φ denote the PPP corresponding to BSs, and let λ be its intensity. BSs transmit at a same power level P_T.

In conventional cellular networks, a user is associated to its nearest BS. Consequently, the resultant cell splitting forms a standard Poisson Voronoi, as shown in Fig. 1(a). Let $\mathbf{T}^{(1)}$ denote the set of cell boundaries in this scenario.

In this paper, we focus on the disjoint cluster mode, where BSs are geographically grouped into fixed clusters. We assume that the plane is covered by a square grid, and each square defines one BS cluster. In other words, all BSs in one square belong to the same cluster. Let $\mathbb{B} = \{(ma + A_1, na + A_2)|m, n \in \mathbb{Z}\}$ denote the set of square centers, where a is the edge length of each square, and A_1 and A_2 are independently uniformly distributed in $[0, a)$. Given an arbitrary point $\mathbf{x}$ on the plane, let $\mathcal{SQ}(\mathbf{x})$ denote the square that $\mathbf{x}$ is located in. In the disjoint cluster mode considered in this work, a

user in the network is firstly associated to its nearest BS. Then, all BSs in the same cluster as the nearest BS will jointly serve the user.

A handoff is defined as the event that the connection BS set of an active user is changed. One major goal of this work is to quantify the rate of handoffs of an active user moving in the network. Therefore, we need to characterize the cluster boundary $\mathbf{T}_0^{(1)}$. We notice that a handoff is made whenever the nearest BS of the user is changed and the new nearest BS is not in the same cluster as the previous nearest BS, so that the connection BS set is changed. As shown in Fig. 1(b), the cluster boundary $\mathbf{T}_0^{(1)}$ corresponds to the set of points, whose distances to two nearest BSs are the same, and the two BSs are not in the same cluster. A handoff is made whenever the user crosses the cluster boundary $\mathbf{T}_0^{(1)}$. Please note that $\mathbf{T}_0^{(1)}$ is a subset of $\mathbf{T}^{(1)}$.

Let $\mathcal{T}_0$ denote the trajectory of the user, which is of finite length. The number of handoffs the user experiences is equal to the number of intersections between $\mathcal{T}_0$ and $\mathbf{T}_0^{(1)}$, which is denoted by $\mathcal{N}(\mathcal{T}_0, \mathbf{T}_0^{(1)})$.

Throughout this paper, we define $\mathcal{B}(\mathbf{x}_0, r)$ as the disk region $\left\{\mathbf{x} \in \mathbb{R}^2 \middle| |\mathbf{x} - \mathbf{x}_0| \leq r\right\}$, and $\overline{\mathcal{B}(\mathbf{x}_0, r)}$ as the region $\mathbb{R}^2 \setminus \mathcal{B}(\mathbf{x}_0, r)$; we define $\mathcal{S}(\mathbf{x}_0, d)$ ($\mathbf{x}_0 = (x_0, y_0)$) as the square region $\left\{(x, y) \in \mathbb{R}^2 \middle| x_0 - \frac{d}{2} \leq x \leq x_0 + \frac{d}{2} \text{ and } y_0 - \frac{d}{2} \leq y \leq y_0 + \frac{d}{2}\right\}$, and $\overline{\mathcal{S}(\mathbf{x}_0, d)}$ as the region $\mathbb{R}^2 \setminus \mathcal{S}(\mathbf{x}_0, d)$.

4 HANDOFF RATE ANALYSIS

In this section, we characterize the handoff rate (the average number of handoffs per unit time) of an active user with an arbitrary movement trajectory. The proposed analysis of handoff rate consists of a progressive sequence of six components, which are described in the following subsections.

4.1 Probability of Two BSs in Different Clusters

First, we consider the probability that two BSs are not in the same cluster, given the distance between them. This is equivalent to a Buffon's needle problem on a square grid [26], which is formally stated in the following lemma.

Lemma 4.1 (Buffon's needle problem on square grid). *Given that a plane is ruled with square grid with square edge length of a, a line segment (e.g., a needle) with length L is randomly placed on the grid, then the probability that the two end points of the line segment are not in the same square (i.e., the line segment is lying across some square edge) is*

$$P(a, L) = 1 - \begin{cases} \frac{a^2\pi + L^2 - 4aL}{a^2\pi}, & \text{if } L < a, \\ \frac{2}{\pi}\left(-1 + 2\sqrt{\frac{L^2}{a^2} - 1} - \frac{L^2}{2a^2} - \arccos\left(\frac{a}{L}\right) + \arcsin\left(\frac{a}{L}\right)\right), & \text{if } a \leq L < \sqrt{2}a, \\ 0, & \text{if } L \geq \sqrt{2}a. \end{cases} \tag{1}$$

Proof. See Appendix A for the proof. □

In the rest of the paper, for simplicity, we define $P_1(a, L) \triangleq 1 - \frac{a^2\pi + L^2 - 4aL}{a^2\pi}$, and $P_2(a, L) \triangleq 1 - \frac{2}{\pi}\Big(-1 + 2\sqrt{\frac{L^2}{a^2} - 1} - \frac{L^2}{2a^2} - \arccos\left(\frac{a}{L}\right) + \arcsin\left(\frac{a}{L}\right)\Big)$.

Lemma 4.1 demonstrates that given L as the distance between two BSs, the probability that they are not in the same cluster is $P(a, L)$ expressed in (1). This important probability will be used in the subsequent handoff analysis.

4.2 Length Intensity of Boundary

Inter-cluster handoffs occur at the intersections of a user's trajectory with $\mathbf{T}_0^{(1)}$. In order to track the number of intersections, we need to express the length intensity of $\mathbf{T}_0^{(1)}$, which is defined as the expected length of $\mathbf{T}_0^{(1)}$ in a unit square.

Following the discussion in Section 3, a point is at $\mathbf{T}_0^{(1)}$ if and only if its distances to two closest BSs are the same and these two BSs do not belong to the same cluster. Mathematically, we have

$$\mathbf{T}_0^{(1)} = \Bigg\{\mathbf{x} \Bigg| \exists \mathbf{x}_1, \mathbf{x}_2 \in \Phi, \mathcal{SQ}(\mathbf{x}_1) \neq \mathcal{SQ}(\mathbf{x}_2), \text{ s.t. } d_r = |\mathbf{x}_1 - \mathbf{x}| = |\mathbf{x}_2 - \mathbf{x}|, \text{and } \forall \mathbf{y} \in \Phi, d_r \leq |\mathbf{y} - \mathbf{x}|\Bigg\}. \tag{2}$$

Please note that the condition $\mathcal{SQ}(\mathbf{x}_1) \neq \mathcal{SQ}(\mathbf{x}_2)$ means that the two closest BSs do not belong to the same cluster so that the user changes cluster. This condition greatly increases the difficulty in the subsequent analysis. Lemma 4.1 will be useful to address this issue.

For reference, we also show the set of cell boundaries $\mathbf{T}^{(1)}$ of the single-BS user association scenario, where users are served by their closest BSs.

$$\mathbf{T}^{(1)} = \Bigg\{\mathbf{x} \Bigg| \exists \mathbf{x}_1, \mathbf{x}_2 \in \Phi, \text{s.t. } d_r = |\mathbf{x}_1 - \mathbf{x}| = |\mathbf{x}_2 - \mathbf{x}|, \text{ and } \forall \mathbf{y} \in \Phi, d_r \leq |\mathbf{y} - \mathbf{x}|\Bigg\}. \tag{3}$$

Note that $\mathbf{T}^{(1)}$ corresponds to the set of cell boundaries of a standard Poisson Voronoi. In Fig. 1(b), $\mathbf{T}_0^{(1)}$ is shown by the thick black lines, and $\mathbf{T}^{(1)}$ is shown by the thin blue lines. We have $\mathbf{T}_0^{(1)} \subseteq \mathbf{T}^{(1)}$.

Let $\mu_1(\mathbf{T}_0^{(1)})$ denote the length intensity of $\mathbf{T}_0^{(1)}$, which is the expected length of $\mathbf{T}_0^{(1)}$ in a unit square:

$$\mu_1(\mathbf{T}_0^{(1)}) = \mathbb{E}\left(\left|\mathbf{T}_0^{(1)} \bigcap [0, 1)^2\right|_1\right), \tag{4}$$

where $|\cdot|_1$ denotes the length (i.e., one-dimensional Lebesgue measure).

4.3 Δd-Extended Boundary and Area Intensity

In order the quantify $\mu_1(\mathbf{T}_0^{(1)})$, we consider the *$\Delta d$-extended boundary*, following a similar step in [10]. The Δd-extended boundary of $\mathbf{T}_0^{(1)}$, denoted by $\mathbf{T}_0^{(2)}(\Delta d)$, is defined as

$$\mathbf{T}_0^{(2)}(\Delta d) = \left\{\mathbf{x} \middle| \exists \mathbf{y} \in \mathbf{T}_0^{(1)}, \text{ s.t. } |\mathbf{x} - \mathbf{y}| < \Delta d\right\}. \tag{5}$$

In other words, $\mathbf{T}_0^{(2)}(\Delta d)$ is the Δd-neighbourhood of $\mathbf{T}_0^{(1)}$.

The area intensity of $\mathbf{T}_0^{(2)}(\Delta d)$ is defined as the expected area of $\mathbf{T}_0^{(2)}(\Delta d)$ in a unit square:

$$\mu_2\big(\mathbf{T}_0^{(2)}(\Delta d)\big) = \mathbb{E}\left(\left|\mathbf{T}_0^{(2)}(\Delta d)\bigcap[0,1)^2\right|_2\right), \tag{6}$$

where $|\cdot|_2$ denotes the area (i.e., two-dimensional Lebesgue measure).

Because $\mathbf{T}_0^{(2)}(\Delta d)$ is stationary, the area intensity of $\mathbf{T}_0^{(2)}(\Delta d)$ is equal to the probability that an arbitrarily located point in the unit square is in $\mathbf{T}_0^{(2)}(\Delta d)$. Thus, we have

$$\mu_2\big(\mathbf{T}_0^{(2)}(\Delta d)\big) = \mathbb{P}(\mathbf{0} \in \mathbf{T}_0^{(2)}(\Delta d)). \tag{7}$$

The probability in (7) is analytically tractable, which will be presented in the next subsection.

Similar to the definitions of $\mu_1\big(\mathbf{T}_0^{(1)}\big)$, $\mathbf{T}_0^{(2)}(\Delta d)$, and $\mu_2\big(\mathbf{T}_0^{(2)}(\Delta d)\big)$, we use the term $\mu_1\big(\mathbf{T}^{(1)}\big)$ to denote the length intensity of $\mathbf{T}^{(1)}$, $\mathbf{T}^{(2)}(\Delta d)$ to denote the Δd-neighbourhood of $\mathbf{T}^{(1)}$, and $\mu_2\big(\mathbf{T}^{(2)}(\Delta d)\big)$ to denote the area intensity of $\mathbf{T}^{(2)}(\Delta d)$. We have $\mu_2\big(\mathbf{T}^{(2)}(\Delta d)\big) = \mathbb{P}(\mathbf{0} \in \mathbf{T}^{(2)}(\Delta d))$.

4.4 Derivation of the Area Intensity

In this subsection, we present the derivation of $\mathbb{P}(\mathbf{0} \in \mathbf{T}_0^{(2)}(\Delta d))$. First, we derive the probability that the reference user at $\mathbf{0}$ is in $\mathbf{T}_0^{(2)}(\Delta d)$, given that its nearest BS is at a distance of $R = r_0$ from it. This conditional probability is derived in the following lemma:

Lemma 4.2. *Let us assume that the reference user is located at $\mathbf{0}$, its nearest BS is R from it. The conditional probability that $\mathbf{0} \in \mathbf{T}_0^{(2)}(\Delta d)$ given $R = r_0$ is*

$$\mathbb{P}(\mathbf{0} \in \mathbf{T}_0^{(2)}(\Delta d)|R = r_0) = 2\Delta d r_0 \lambda * \int_0^{\pi} \sqrt{2-2\cos(\theta)}P(a, r_0\sqrt{2-2\cos(\theta)})\mathrm{d}\theta + O(\Delta d^2). \tag{8}$$

Proof. See Appendix B for the proof. □

From [21], we know that the probability density function (pdf) of the distance between the reference user and its closet BS R is

$$f(r_0) = 2\pi\lambda r_0 \exp(-\lambda\pi r_0^2). \tag{9}$$

Consequently, we can derive the unconditioned probability of $\mathbf{0} \in \mathbf{T}_0^{(2)}(\Delta d)$ through deconditioning on R,

$$\mathbb{P}(\mathbf{0} \in \mathbf{T}_0^{(2)}(\Delta d)) = \int_0^{\infty} f(r_0)\mathbb{P}(\mathbf{0} \in \mathbf{T}_0^{(2)}(\Delta d)|R = r_0)\mathrm{d}r_0. \tag{10}$$

4.5 Length Intensity

Following Section 3.2 in [16], we can derive the length intensity $\mu_1\big(\mathbf{T}_0^{(1)}\big)$ directly from the area intensity $\mu_2\big(\mathbf{T}_0^{(2)}(\Delta d)\big)$ as follows

$$\mu_1\big(\mathbf{T}_0^{(1)}\big) = \lim_{\Delta d \to 0} \frac{\mu_2\big(\mathbf{T}_0^{(2)}(\Delta d)\big)}{2\Delta d}. \tag{11}$$

Through (7)–(11), we can derive the length intensity, formally stated in the following theorem:

Theorem 4.3. *The length intensity $\mu_1\big(\mathbf{T}_0^{(1)}\big)$ is expressed as*

$$\mu_1\big(\mathbf{T}_0^{(1)}\big) = \int_0^{\infty} 2\pi\lambda^2 r_0^2 \exp(-\lambda\pi r_0^2)\cdot \int_0^{\pi} \sqrt{2-2\cos(\theta)}P(a, r_0\sqrt{2-2\cos(\theta)})\mathrm{d}\theta\mathrm{d}r_0. \tag{12}$$

By investigating the derived length intensity, we observe its two important properties.

4.5.1 Scaling Property. Expression (12) shows that $\mu_1\big(\mathbf{T}_0^{(1)}\big)$ depends only on the density of BSs λ and the edge length of cluster a. Therefore, let $\mu(a,\lambda) \triangleq \mu_1\big(\mathbf{T}_0^{(1)}\big)$ under a and λ. After mathematical manipulations, we can observe the following scaling property of $\mu(a,\lambda)$ as follows.

Corollary 4.4 (Scaling property of length intensity). *Given $A > 0$, we have*

$$\mu(a,\lambda) = \mu(Aa, \frac{\lambda}{A^2})\cdot A. \tag{13}$$

Proof.

$$\mu(Aa, \frac{\lambda}{A^2}) \tag{14}$$

$$= \int_0^{\infty} 2\pi\frac{\lambda^2}{A^4} r_0^2 \exp(-\frac{\lambda}{A^2}\pi r_0^2)\cdot \int_0^{\pi} \sqrt{2-2\cos(\theta)}P(Aa, r_0\sqrt{2-2\cos(\theta)})\mathrm{d}\theta\mathrm{d}r_0 \tag{15}$$

$$= \int_0^{\infty} 2\pi\frac{\lambda^2}{A^2} r_1^2 \exp(-\lambda\pi r_1^2)\cdot A\int_0^{\pi} \sqrt{2-2\cos(\theta)}P(Aa, Ar_1\sqrt{2-2\cos(\theta)})\mathrm{d}\theta\mathrm{d}r_1 \tag{16}$$

$$= \frac{1}{A}\int_0^{\infty} 2\pi\lambda^2 r_1^2 \exp(-\lambda\pi r_1^2)\cdot \int_0^{\pi} \sqrt{2-2\cos(\theta)}P(a, r_1\sqrt{2-2\cos(\theta)})\mathrm{d}\theta\mathrm{d}r_1 \tag{17}$$

$$= \frac{1}{A}\mu(a,\lambda). \tag{18}$$

where (15) follows the expression of (12); (16) is derived through setting $r_0 = Ar_1$; and (17) is by noting that $P(a, L) = P(Aa, AL)$ (see the definition in (1)). □

4.5.2 Asymptotical Property. It is also interesting to show the asymptotical property of the length intensity when $\lambda a^2 \gg 1$. It corresponds to the practical scenario where each cluster comprises many BSs. We notice that the outer level integration of (12) can be partitioned into $\int_0^{\frac{a}{2}}(\cdot)\mathrm{d}r_0$ and $\int_{\frac{a}{2}}^{\infty}(\cdot)\mathrm{d}r_0$ regions. In the $\int_0^{\frac{a}{2}}(\cdot)\mathrm{d}r_0$ region, $r_0\sqrt{2-2\cos(\theta)}$ is no grater than a, and thus $P(a, r_0\sqrt{2-2\cos(\theta)}) = P_1(a, r_0\sqrt{2-2\cos(\theta)})$. In the $\int_{\frac{a}{2}}^{\infty}(\cdot)\mathrm{d}r_0$ region, when λa^2 is large (λr_0^2 is large), $\exp(-\lambda\pi r_0^2)$ is small. Thus, $\int_{\frac{a}{2}}^{\infty} 2\pi\lambda^2 r_0^2 \exp(-\lambda\pi r_0^2)\int_0^{\pi}\sqrt{2-2\cos(\theta)}P(a, r_0\sqrt{2-2\cos(\theta)})\mathrm{d}\theta\mathrm{d}r_0 \simeq 0 \simeq \int_{\frac{a}{2}}^{\infty} 2\pi\lambda^2 r_0^2 \exp(-\lambda\pi r_0^2)\int_0^{\pi}\sqrt{2-2\cos(\theta)}P_1(a, r_0\sqrt{2-2\cos(\theta)})\mathrm{d}\theta\mathrm{d}r_0$. Therefore, $P(a, r_0\sqrt{2-2\cos(\theta)})$ can be replaced by $P_1(a, r_0\cdot\sqrt{2-2\cos(\theta)})$ in this region as they are asymptotically equivalent.

As a consequence, when $\lambda a^2 \gg 1$, we have

$$\mu(a,\lambda) = \int_0^\infty 2\pi\lambda^2 r_0^2 \exp(-\lambda\pi r_0^2)\cdot \int_0^\pi \sqrt{2-2\cos(\theta)}P(a, r_0\sqrt{2-2\cos(\theta)})\mathrm{d}\theta\mathrm{d}r_0 \quad (19)$$

$$\simeq \int_0^\infty 2\pi\lambda^2 r_0^2 \exp(-\lambda\pi r_0^2)\cdot \int_0^\pi \sqrt{2-2\cos(\theta)}P_1(a, r_0\sqrt{2-2\cos(\theta)})\mathrm{d}\theta\mathrm{d}r_0 \quad (20)$$

$$= \frac{8\left(\pi a\sqrt{\lambda}-1\right)\sqrt{\lambda}}{a^2\lambda\pi^2} \triangleq \widetilde{\mu}(a,\lambda), \quad (21)$$

so that the closed-form expression (21) shows the asymptotical length intensity of the cluster boundaries.

In Section 6, we will further show that (21) is accurate even if λa^2 is not large. In addition, the closed-form expression (21) will facilitate the design of the optimal cluster size, which will be discussed in Section 5.3.

4.6 Handoff Rate

Let $\mathcal{T}_0$ denote an arbitrary user's trajectory on $\mathbb{R}^2$ with length D. Then, the expected number of intersections of $\mathcal{T}_0$ and $\mathbf{T}_0^{(1)}$ is $\frac{2}{\pi}\mu_1(\mathbf{T}_0^{(1)})D = \frac{2}{\pi}\mu(a,\lambda)D$ [34]. Let v denote the instantaneous velocity of the active user; then its inter-cluster handoff rate (i.e., expected number of handoffs per unit time) is

$$\frac{2}{\pi}\mu_1(\mathbf{T}_0^{(1)})v = \frac{2}{\pi}\mu(a,\lambda)v. \quad (22)$$

5 DOWNLINK DATA RATE ANALYSIS AND OPTIMAL CLUSTER SIZE

In this section, as a study on the application of the above handoff rate analysis, we first quantify the downlink user data rate under the NC-JT scheme. Then, we investigate the optimal cluster size that balances the handoff rate and the data rate. Note that we focus on the NC-JT scheme because it is one of the most commonly adopted cooperative transmission schemes in practical systems [1], and it is easily implemented since a tight synchronization of joint signal transmission is not required [35].

We assume that each user and BS is equipped with a single antenna. Each BS transmits at power level P_T. If a BS is located at $\mathbf{x}$, then the received power at $\mathbf{y}$ is $\frac{P_T h_{\mathbf{x},\mathbf{y}}}{|\mathbf{x}-\mathbf{y}|^\alpha}$, where $\alpha > 2$ is the pathloss exponent, $|\mathbf{x}-\mathbf{y}|^\alpha$ is the propagation loss function, and $h_{\mathbf{x},\mathbf{y}}$ is the normalized fast fading term. Corresponding to common Rayleigh fading with power normalization, $h_{\mathbf{x},\mathbf{y}}$ is independently exponentially distributed with unit mean. Also, we have assumed the system is interference limited, such that noise is negligible.

5.1 Data Rate Analysis

We aim to derive the average downlink user data rate via stochastic geometric analysis. We consider a reference user. Its closest BS is referred to as the reference BS. According to Section 3, all BSs in the same cluster as the reference BS are the serving BSs of the reference user. All BSs not in the same cluster as the reference BS are non-cooperative BSs. We focus on the reference user since the average data rate performance in the system is the same as the performance of the reference user. Furthermore, due to the stationarity of users and BSs, throughout this section we will re-define the coordinates so that the reference user is located at $\mathbf{0}$. Without loss of generality, we assume that the user operates on a unit frequency bandwidth.

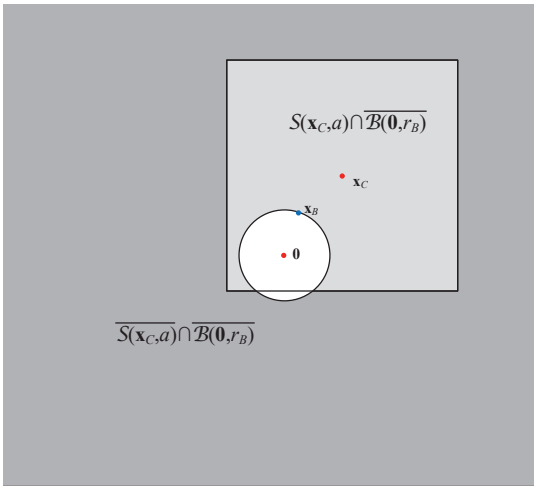

Figure 2: The light grey region shows $\mathcal{S}(\mathbf{x}_C,a)\bigcap\overline{\mathcal{B}(\mathbf{0},r_B)}$, in which the cooperative BSs are random distributed. The dark grey region shows $\overline{\mathcal{S}(\mathbf{x}_C,a)}\bigcap\overline{\mathcal{B}(\mathbf{0},r_B)}$, in which the non-cooperative BSs are random distributed.

Following the discussion in [27, 35], under NC-JT, the signal-to-interference ratio (SIR) at the reference user is expressed as

$$\mathrm{SIR} = \frac{\sum_{\mathbf{x}\in\Phi_{in}}|\mathbf{x}|^{-\alpha}h_{\mathbf{x},\mathbf{0}}}{\sum_{\mathbf{x}\in\Phi_{out}}|\mathbf{x}|^{-\alpha}h_{\mathbf{x},\mathbf{0}}}, \quad (23)$$

where Φ_{in} corresponds to the point process of all cooperative BSs (i.e., all BSs in the same cluster as the reference BS), and Φ_{out} corresponds to the point process of the other non-cooperative (interfering) BSs. We further define $S \triangleq \sum_{\mathbf{x}\in\Phi_{in}}|\mathbf{x}|^{-\alpha}h_{\mathbf{x},\mathbf{0}}$ as the received signal power from the cooperative BSs, and $I \triangleq \sum_{\mathbf{x}\in\Phi_{out}}|\mathbf{x}|^{-\alpha}h_{\mathbf{x},\mathbf{0}}$ as the sum interference generated by non-cooperative BSs.

Let $\mathbf{X}_B = (X_B, Y_B)$ denote the Cartesian coordinate of the reference BS and $\mathbf{R}_B = (R_B, \Theta_B)$ denote its polar coordinate. X_B, Y_B, R_B, and Θ_B are random variables. We have $X_B = R_B\cos\Theta_B$ and $Y_B = R_B\sin\Theta_B$. The pdf of (R_B, Θ_B) is then derived as follows [21].

$$\mathrm{pdf}_{R_B,\Theta_B}(r,\theta) = r\lambda\exp(-\pi\lambda r^2),\ r\geq 0,\ 0\leq\theta<2\pi. \quad (24)$$

Given the reference BS's coordinate (Cartesian coordinate $\mathbf{X}_B = \mathbf{x}_B = (x_B, y_B)$ and polar coordinate $\mathbf{R}_B = \mathbf{r}_B = (r_B, \theta_B)$), all other BS coordinates correspond to the Palm point process of Φ, denoted by Φ'. It can be shown that Φ' is a PPP with intensity 0 in the disk region $\mathcal{B}(\mathbf{0}, r_B)$ and intensity λ in $\overline{\mathcal{B}(\mathbf{0}, r_B)}$.

Given the coordinate of the reference BS, we also need to determine the distribution of the coordinate of the center of the cluster to which the reference BS belongs, denoted by $\mathbf{X}_C$. Since BSs are homogeneously distributed in the cluster, given the location of the reference BS, the cluster center is uniformly distributed in the square region $\mathcal{S}(\mathbf{x}_B, a)$ (i.e, the square centered at $\mathbf{x}_B$ with edge length a) [5, Page 60]. Equivalently, the pdf of $\mathbf{X}_C$ given the polar

coordinate of the reference BS (r_B, θ_B) is then expressed as follows

$$\mathrm{pdf}_{\mathbf{X}_C|(r_B,\theta_B)}(x,y) = \frac{1}{a^2}, \tag{25}$$

$$r_B\cos\theta_B - \frac{a}{2} \le x < r_B\cos\theta_B + \frac{a}{2}, \tag{26}$$

$$r_B\sin\theta_B - \frac{a}{2} \le y < r_B\sin\theta_B + \frac{a}{2}. \tag{27}$$

Given both the polar coordinate of the reference BS $\mathbf{r}_B = (r_B, \theta_B)$ and the Cartesian coordinate of the cluster center $\mathbf{x}_C = (x_C, y_C)$, we can notice that a BS in the square region $\mathcal{S}(\mathbf{x}_C, a)$ is a cooperative BS and a BS in $\overline{\mathcal{S}(\mathbf{x}_C, a)}$ is a non-cooperative interfering BS of the reference user. Therefore, $\Phi'_{in} = \Phi' \bigcap \mathcal{S}(\mathbf{x}_C, a)$ corresponds to all cooperative BSs except for the reference BS, and $\Phi_{out} = \Phi' \bigcap \overline{\mathcal{S}(\mathbf{x}_C, a)}$ corresponds to all non-cooperative interfering BSs. The set of all cooperative BSs is $\Phi_{in} = \Phi'_{in} \bigcup \mathbf{x}_B$. As a consequence, we can derive the Laplace transform of the signal strength given $\mathbf{R}_B = \mathbf{r}_B$ and $\mathbf{X}_C = \mathbf{x}_C$ (denoted by $\mathcal{L}_{S|\mathbf{r}_B,\mathbf{x}_C}(s)$) as follows

$$\mathcal{L}_{S|\mathbf{r}_B,\mathbf{x}_C}(s) = \mathbb{E}\left(e^{-sS}\middle|\mathbf{R}_B = \mathbf{r}_B, \mathbf{X}_C = \mathbf{x}_C\right) \tag{28}$$

$$= \mathbb{E}\left(e^{-s\left(\frac{h_{\mathbf{x}_B,\mathbf{0}}}{r_B^{\alpha}} + \sum_{\mathbf{x}\in\Phi'_{in}} \frac{h_{\mathbf{x},\mathbf{0}}}{|\mathbf{x}|^{\alpha}}\right)}\middle|\mathbf{R}_B = \mathbf{r}_B, \mathbf{X}_C = \mathbf{x}_C\right) \tag{29}$$

$$= \frac{1}{1+\frac{s}{r_B^{\alpha}}} \cdot \exp\left(-\lambda \int_{\mathcal{S}(\mathbf{x}_C,a)\cap\overline{\mathcal{B}(\mathbf{0},r_B)}} \frac{s}{s+|\mathbf{x}|^{\alpha}}\mathrm{d}\mathbf{x}\right), \tag{30}$$

where (30) follows the definition of the Laplace functional of a PPP and is because h terms are independently exponentially distributed. Similarly, the Laplace transform of sum interference given $\mathbf{R}_B = \mathbf{r}_B$ and $\mathbf{X}_C = \mathbf{x}_C$ (denoted by $\mathcal{L}_{I|\mathbf{r}_B,\mathbf{x}_C}(s)$) can be derived as follows

$$\mathcal{L}_{I|\mathbf{r}_B,\mathbf{x}_C}(s) = \mathbb{E}\left(e^{-sI}\middle|\mathbf{R}_B = \mathbf{r}_B, \mathbf{X}_C = \mathbf{x}_C\right) \tag{31}$$

$$= \mathbb{E}\left(e^{-s\left(\sum_{\mathbf{x}\in\Phi_{out}} \frac{h_{\mathbf{x},\mathbf{0}}}{|\mathbf{x}|^{\alpha}}\right)}\middle|\mathbf{R}_B = \mathbf{r}_B, \mathbf{X}_C = \mathbf{x}_C\right) \tag{32}$$

$$= \exp\left(-\lambda \int_{\overline{\mathcal{S}(\mathbf{x}_C,a)}\cap\overline{\mathcal{B}(\mathbf{0},r_B)}} \frac{s}{s+|\mathbf{x}|^{\alpha}}\mathrm{d}\mathbf{x}\right). \tag{33}$$

Now that we have derived the Laplace transforms of the signal and interference, the data rate of the reference user (given $\mathbf{R}_B = \mathbf{r}_B$ and $\mathbf{X}_C = \mathbf{x}_C$) can be computed as (34). Note that the derivation of (34) follows Lemma 1 of [25].

$$\mathrm{R}(\mathbf{r}_B, \mathbf{x}_C) = \int_0^{\infty} \frac{1}{s}\mathcal{L}_{I|\mathbf{r}_B,\mathbf{x}_C}(s)(1 - \mathcal{L}_{S|\mathbf{r}_B,\mathbf{x}_C}(s))\mathrm{d}s. \tag{34}$$

By combining (24), (25), and (34), as well as the law of total probability, we can finally derive the unconditioned average data rate of the reference user as follows

$$\mathrm{R} = \int_0^{\infty}\int_0^{2\pi}\int_{\mathcal{S}((r_B\cos\theta_B, r_B\sin\theta_B),a)} \mathrm{pdf}_{R_B,\Theta_B}(r_B,\theta_B)\cdot \mathrm{pdf}_{\mathbf{X}_C|r_B,\theta_B}(\mathbf{x}_C)\mathrm{R}((r_B,\theta_B),\mathbf{x}_C)\mathrm{d}\mathbf{x}_C\mathrm{d}\theta_B\mathrm{d}r_B. \tag{35}$$

Since R depends on λ and a, R is written as $\mathrm{R}(a,\lambda)$ in the rest of this paper.

5.2 Scaling Property of Data Rate

Please notice that since we consider an interference limited scenario, the average data rate is invariant if we simultaneously change λ to $\frac{\lambda}{A^2}$ and a to aA, due to the scaling property of the SIR (Section 16.2.4 of [6]).[2] For positive values of A, we have

$$\mathrm{R}(a,\lambda) = \mathrm{R}(Aa, \frac{\lambda}{A^2}). \tag{36}$$

Please also note that the scaling property of $\mathrm{R}(a,\lambda)$ in (36) is different to the scaling property of $\mu(a,\lambda)$ in (13). This is because the SIR is invariant (i.e., a ratio of signal power and interference, both of which are multiplied by the same factor $\frac{1}{A^{\alpha}}$) if we re-scale the plane $\mathbb{R}^2$. A significant distinction in (13) is that if we re-scale the plane $\mathbb{R}^2$, the set of boundaries is geometrically similar rather than congruent to its original shape, and thus its one-dimensional Lebesgue measure changes (multiplied by a factor of $\frac{1}{A}$).

In this section, the derived data rate expression is not in a closed form, but given as an integral with a few levels of integrations. This is inevitable due to the stochastic geometric analysis. Numerical computation of multiple levels of integrations may be time-consuming. However, computations can be simplified by the scaling property shown in (36): we only need to compute the values of $\mathrm{R}(a,1)$ for different a once, in an *offline* fashion. Then, these values can be reused when we characterize systems with different BS densities, through applying the formula $\mathrm{R}(a,\lambda) = \mathrm{R}(a\sqrt{\lambda},1)$.

5.3 Case Study: Optimal Cluster Size

In this subsection, we present an application scenario of our proposed handoff and data rate analyses. We aim to design the optimal edge length a under a given BS intensity λ in order to calculate a tradeoff between the data rate and handoff cost. For convenience, we define $K \triangleq a^2\lambda$ as the cluster size (the average number of BSs per cluster). Equivalently, we consider the optimal cluster size K under different λ.

In order to quantify the tradeoff between the user date rate and handoff rate, we consider their weighted sum. We notice that under different cluster sizes K, different numbers of BSs will be involved in one handoff event. As a consequence, the cost of one handoff differs under different K. To properly compare handoffs under different K, we assume that the cost of one handoff is proportional to the expected number of BSs involved during one handoff event. On average, K BSs are disconnected and K BSs are connected, leading to a cost of $2KW_1$, where W_1 is an arbitrary weight value. Therefore, by combining (13) and (22), the average handoff cost per unit time is computed as

$$H(K) = W_1\mu(a,\lambda)\cdot\frac{2}{\pi}v\cdot 2K \tag{37}$$

$$= W_1\mu(a\sqrt{\lambda},1)\sqrt{\lambda}\cdot\frac{2}{\pi}v\cdot 2K \tag{38}$$

$$= W_1\mu(\sqrt{K},1)\sqrt{\lambda}\cdot\frac{2}{\pi}v\cdot 2K. \tag{39}$$

Then, let W_2 be the utility value for one bit of data transmission, the average utility (gained from data transfer) per unit time is computed as

$$L(K) = W_2\mathrm{R}(a,\lambda) = W_2\mathrm{R}(a\sqrt{\lambda},1) = W_2\mathrm{R}(\sqrt{K},1). \tag{40}$$

[2] If we relocate every BS $\mathbf{x} \in \Phi$ to $A\mathbf{x}$ as well as multiply the cluster edge length a by a factor of A, we derive a network with BS intensity $\frac{\lambda}{A^2}$ and cluster edge length aA, but the same SIR since both the numerator and denominator of SIR (in (23)) is multiplied by a factor of $\frac{1}{A^{\alpha}}$, compared with the original network.

Table 1: Values of B and β under different α.

α value	B value	β value	Coefficient of determination
2.5	0.77	6.21	0.9974
3.0	1.11	5.45	0.9985
3.5	1.46	5.20	0.9988
4.0	1.81	5.10	0.9988
4.5	2.14	5.06	0.9988

Consequently, the overall average utility per unit time is computed as a weighted sum of handoff cost and user data rate

$$U(K) = W_2 \mathrm{R}(\sqrt{K}, 1) - W_1 \mu(\sqrt{K}, 1)\sqrt{\lambda} \cdot \frac{2}{\pi} v \cdot 2K. \tag{41}$$

A straightforward way to find the optimal K is through a numerical search method by combining (12), (35), and (41). However, that method does not give much insight on how different parameters influence the optimal K. In this subsection, we are more interested to evaluate an approximated optimal value K in a closed form. We resort to approximation approaches as follows.

We employ the asymptotical value of $\mu(\sqrt{K}, 1)$, i.e., $\widetilde{\mu}(\sqrt{K}, 1)$ in (21) to approximate $\mu(\sqrt{K}, 1)$. This is because even when $K = \lambda a^2$ is not large, $\widetilde{\mu}(\sqrt{K}, 1)$ can still provide a good approximation to $\mu(\sqrt{K}, 1)$ (as shown later in Section 6). Therefore, by considering (21), we have

$$H(K) \simeq W_1 \frac{32(\pi\sqrt{K} - 1)\sqrt{\lambda}}{\pi^3} v. \tag{42}$$

Next, we consider the term $\mathrm{R}(\sqrt{K}, 1)$. Let $\widehat{\mathrm{R}}(K) \triangleq \mathrm{R}(\sqrt{K}, 1)$. Due to the scaling property discussed in Section 5.2, we only need to characterize $\widehat{\mathrm{R}}(K)$ once, even for different λ. We resort to numerical evaluation of $\widehat{\mathrm{R}}(K)$, and then find that $\widehat{\mathrm{R}}(K)$ can be closely approximated as

$$\widehat{\mathrm{R}}(K) \approx B \sqrt[\beta]{K}, \tag{43}$$

where B and β are fit parameters. Table 1 shows the values of B and β under different α values (i.e., pathloss exponent). In this step, (43) is equivalent to $\ln(\widehat{\mathrm{R}}) = \ln B + \frac{1}{\beta} \ln(K)$. Through conducting linear regression between the numerical values of $\ln(\widehat{\mathrm{R}})$ and $\ln(K)$, we can compute B and β under different α values.[3] In all cases, the coefficients of determination (R squared values) [36] of linear regression are all above 0.995, indicating the accuracy of the approximation formula $\ln(\widehat{\mathrm{R}}) = \ln B + \frac{1}{\beta} \ln(K)$. The level of goodness-of-fit is very high.

By combining (42) and (43), we have

$$U(K) \approx -W_1 \frac{32(\pi\sqrt{K} - 1)\sqrt{\lambda}}{\pi^3} v + W_2 B \sqrt[\beta]{K}. \tag{44}$$

By taking the first-order derivative, (44) is optimized when K equals to

$$K^* = \sqrt[(\frac{1}{2} - \frac{1}{\beta})]{\frac{\pi^2 W_2 B}{16 W_1 \sqrt{\lambda} v \beta}}, \tag{45}$$

which is an approximated optimal value of K in a closed form. In Section 6, we will further show that (45) is accurate under a variety of parameter settings.

[3] During the linear regression, K is set to be an integer and it ranges from 1 to 50.

6 SIMULATION

In this section, we present simulation results to validate our proposed new analyses. In each round of simulation, BSs are generated on a 20 km × 20 km square. Then, we randomly generate 6 waypoints $\mathbf{X}_1, \mathbf{X}_2, \ldots, \mathbf{X}_6$ in the central 10 km × 10 km square. The five line segments $\mathbf{X}_1\mathbf{X}_2, \mathbf{X}_2\mathbf{X}_3, \ldots, \mathbf{X}_5\mathbf{X}_6$ form the trajectory of an active user in one round of simulation. Each data point is averaged over 10000 simulation rounds. Throughout this section, we assume that the user operates on a unit frequency bandwidth 1 MHz. BS transmission power is set to be 46 dBm.

6.1 Handoff Rate

First, we validate the proposed handoff rate analysis presented in Section 4. We compare the simulated handoff rate, exact analytical handoff rate, and the asymptotical handoff rate expressed in (21) in Fig. 3(a). The λ and a values are indicated in the figure, and v is set to be 10 km/h. The figure shows that the simulated handoff rates match the exact analytical rates, validating the correctness of the handoff analysis. In addition, the asymptotical handoff rates approach to exact analytical rates, when λa^2 increases, verifying the asymptotical property discussed in Section 4.5.2. In addition, the asymptotical values are close to exact values even if λa^2 is not large, so that the asymptotical handoff rates expressed in closed form can be employed to well estimate the exact handoff rates expressed in non-closed form.

Then, we validate the scaling property of handoff rate presented in Corollary 4.4. Following (13), we have $\mu(\sqrt{\frac{K}{\lambda}}, \lambda) = \mu(\sqrt{\frac{K}{\lambda}} \cdot \sqrt{\lambda}, \lambda \cdot \frac{1}{\sqrt{\lambda^2}}) \cdot \sqrt{\lambda}$, and thus $\frac{\mu(\sqrt{\frac{K}{\lambda}}, \lambda)}{\sqrt{\lambda}} = \mu(\sqrt{K}, 1)$. In Fig. 3(b), by fixing K (i.e., $a^2\lambda$), we aim to verify if $\frac{\mu(\sqrt{\frac{K}{\lambda}}, \lambda)}{\sqrt{\lambda}}$ is constant under different λ. We show the simulated values of handoff rate over square root of λ (i.e., $\frac{\mu(\sqrt{\frac{K}{\lambda}}, \lambda)}{\sqrt{\lambda}}$), under different λ but a constant K. We also show the analytical value of $\frac{\mu(\sqrt{\frac{K}{\lambda}}, \lambda)}{\sqrt{\lambda}}$ for reference. In the simulation, v is set to be 10 km/h. As a consequence, Fig. 3(b) shows that the simulated $\frac{\mu(\sqrt{\frac{K}{\lambda}}, \lambda)}{\sqrt{\lambda}}$ is indeed a constant, and is the same as the analytical result, validating the correctness of the scaling property of the handoff rate.

6.2 Data Rate

In Fig. 3(c), we show the data rates under different K. a is set to be 1 km, and α is set to be 4. The figure validates that the analytical data rates match with simulated data rates, and the approximated data rates by employing (43) are also very close to the real data rates. This confirms that (43) can be employed to further characterize the optimal cluster shown in (44)–(45).

In Fig. 3(d), we validate the scaling property of the data rate shown in (36). We show the data rates under different λ values

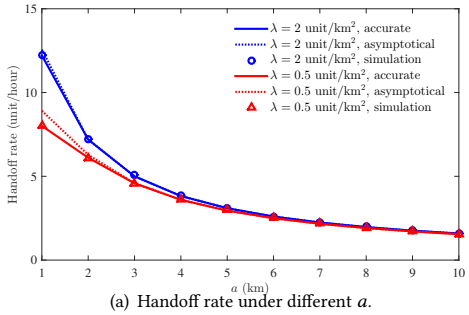

(a) Handoff rate under different a.

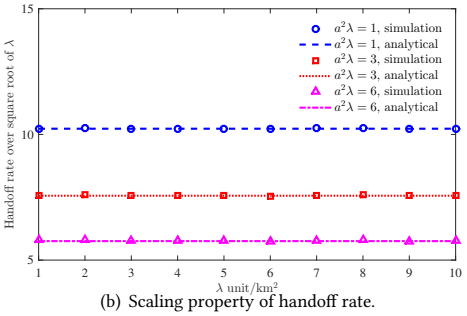

(b) Scaling property of handoff rate.

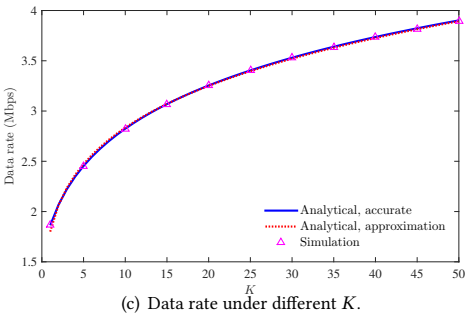

(c) Data rate under different K.

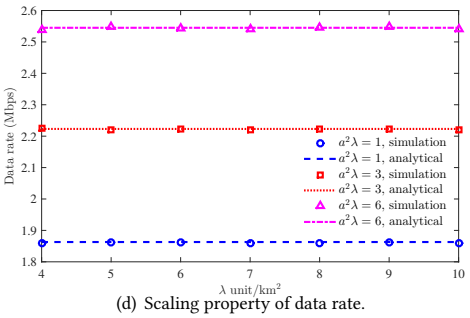

(d) Scaling property of data rate.

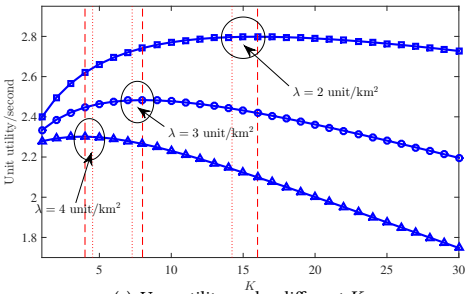

(e) User utility under different K.

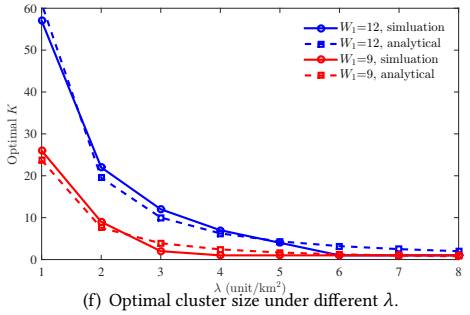

(f) Optimal cluster size under different λ.

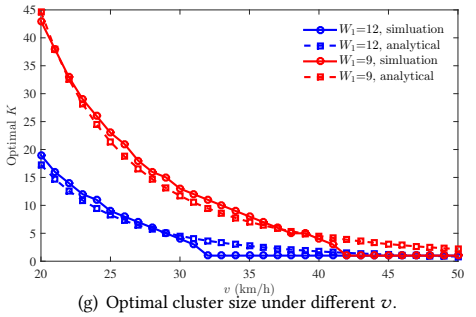

(g) Optimal cluster size under different v.

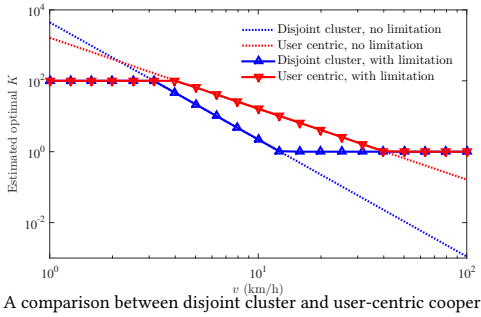

(h) A comparison between disjoint cluster and user-centric cooperation.

Figure 3: Evaluation results.

when λa^2 is fixed. α is set to be 4. The figure shows that the data rate is indeed a constant if we fix λa^2, validating the correctness of the scaling property of the data rate.

6.3 Optimal Cluster Size

In Fig. 3(e), we present the simulated user utility $U(K)$ under different values of the cluster size K. The network parameters are as follows: $\alpha = 4$, $W_1 = 10$, $W_2 = 1$, and $v = 36$ km/h. The simulated results are plotted for $\lambda = 2$, 3, and 4 unit/km^2 respectively. The dashed vertical lines show the optimal K (as integer values)

by simulation, and the dotted vertical lines show the K^* values derived by (45). The results validate that the simulated optimal solutions are close to those derived in (45), illustrating the usefulness of expression (45) to approximate the optimal cluster size K.

In Fig. 3(f), we consider the optimal cluster size K under different BS intensity λ, and in Fig. 3(g), we present the optimal K under different user velocities v. In these figures, we set $\alpha = 4$, and $W_2 = 1$. In Fig. 3(f), we set $v = 36$ km/h, and in Fig. 3(g), we set $\lambda = 4$ unit/km^2. We assume that the cluster size is at least one in these scenarios. The figures validate that the optimal cluster sizes derived by (45) are close to the simulated optimal cluster sizes under a wide range of user velocities and BS intensities. In addition, the figure suggests that the optimal cluster size decreases if the BS intensity λ or the user velocity v increases.

6.4 Comparison with the User-Centric Case

Finally, we also compare the optimal cluster size between disjoint-clustered BS cooperation, which is our focus, and user-centric BS cooperation discussed in [11]. We base the comparisons on (45) for our approach and expression (28) in [11], as (45) closely approximates the optimal cluster size for disjoint-clustered BS cooperation, and (28) in [11] gives the optimal cluster size for user-centric BS cooperation. Furthermore, in order to properly compare these two modes, we set the cost of one handoff in the user-centric mode as $2W_1$ since only two BSs are involved (one is connected and the other is disconnected) when a handoff occurs in this scenario (in contrast to that $2K$ BSs are involved in the disjoint-cluster scenario). The network parameters are as follows: $\alpha = 4$, $W_1 = 40$, $W_2 = 1$, $\lambda = 5$ unit/km^2, and $v = 36$ km/h.

The comparison between the two modes are shown in Fig. 3(h). The dotted lines show the results from (45) in this paper and expression (28) in [11] respectively. We note that these analytical expressions may lead to arbitrarily large cluster sizes, while cluster sizes are limited in reality. We thus consider a maximum and a minimum possible cluster size, 100 and 1 respectively, for demonstration purpose. The results are shown by the solid curves. Please also note the x-axis and y-axis are in log scale in this figure. From the analysis, we can observe that the optimal cluster size is inversely proportional to v^2 in the user-centric mode, but inversely proportional to $v^{\frac{1}{\frac{1}{2}-\frac{1}{\beta}}}$ (where $\frac{1}{\frac{1}{2}-\frac{1}{\beta}}$ is greater than 2). As a consequence, the slope of the blue dotted line is steeper than that of the red dotted line. When we further constrain the cluster size in $[1, 100]$, the optimal cluster size in the user-centric mode is no smaller than that in the disjoint-clustered mode in Fig. 3(h), suggesting that a larger cluster size is favored in the user-centric mode.

7 CONCLUSIONS

In this paper, we provide a theoretical framework to analyze the handoffs in disjoint-clustered cooperative wireless networks. Through the proposed stochastic geometric analysis, we capture the irregularly shaped network topology introduced by irregularly distributed BSs (caused by emerging technologies). The analytical expression for the handoff rate experienced by an active user with arbitrary movement trajectory is derived. We also calculate the average downlink data rate of users under the non-coherent joint-transmission (NC-JT) scheme. The derived expression of the data rate is in a form of an integral with a few levels of integrations, and it is approximated by a simple expression in a closed form. Based on the above analyses, we propose an optimal cluster size formulation considering both the handoff rate and the data rate, where the optimal cluster size can be estimated by a simple closed-form expression, which indicates that the optimal cluster size decreases if the BS intensity or the user velocity increases. Extensive simulations are conducted, validating the correctness and usefulness of our analytical results.

APPENDIX

7.1 Proof of Lemma 4.1

Proof. As shown in Fig. 4: Let $\mathbf{o}$ be the center of the needle. Let X be the distance from $\mathbf{o}$ to the its left closest vertical line, Y be the distance from $\mathbf{o}$ to its top closest horizontal line, and Θ be the angle between the needle and the horizontal lines. X and Y are independently uniformly distributed between 0 and a; Θ is uniformly distributed between 0 and π.

Given $\Theta = \theta$, then the probability that the needle does not cross vertical lines is

$$\begin{aligned} p_v(\theta) =& \mathbb{P}\left(X - \frac{L|\cos\theta|}{2} \geq 0, X + \frac{L|\cos\theta|}{2} < a\right) \\ =& \begin{cases} 1 - \frac{L|\cos\theta|}{a}, & \text{if } L|\cos\theta| \leq a, \\ 0, & \text{if } L|\cos\theta| > a. \end{cases} \end{aligned} \tag{46}$$

The probability that the needle does not cross horizontal lines is

$$\begin{aligned} p_h(\theta) =& \mathbb{P}\left(\frac{Y - L\sin\theta}{2} \geq 0, Y + \frac{L\sin\theta}{2} < a\right) \\ =& \begin{cases} 1 - \frac{L\sin\theta}{a}, & \text{if } L\sin\theta \leq a, \\ 0, & \text{if } L\sin\theta > a. \end{cases} \end{aligned} \tag{47}$$

Finally, the probability that the needle does not cross any line is

$$P_N(a, L) = \frac{1}{\pi}\int_0^{\pi} p_v(\theta)p_h(\theta)\mathrm{d}\theta \tag{48}$$

$$= \begin{cases} \frac{a^2\pi + L^2 - 4aL}{a^2\pi}, & \text{if } L < a, \\ \frac{2}{\pi}\left(-1 + 2\sqrt{\frac{L^2}{a^2} - 1} - \frac{L^2}{2a^2} - \arccos\left(\frac{a}{L}\right) + \arcsin\left(\frac{a}{L}\right)\right), & \\ & \text{if } a \leq L < \sqrt{2}a, \\ 0, & \text{if } L \geq \sqrt{2}a. \end{cases}$$

Finally, we have $P(a, L) = 1 - P_N(a, L)$, which completes the proof. □

7.2 Proof of Lemma 4.2

Proof. In this proof, the BS closest to the reference user is referred to as the reference BS. Without loss of generality, we assume the reference BS is located at $\mathbf{r}_0 = (r_0, 0)$. Note that there are no BSs located within $\mathcal{B}(\mathbf{0}, r_0)$, where $\mathcal{B}(\mathbf{x}, r)$ denotes the disk region centered at $\mathbf{x}$ with radius r, and $\overline{\mathcal{B}(\mathbf{x}, r)}$ denotes $\mathbb{R}^2 \setminus \mathcal{B}(\mathbf{x}, r)$.

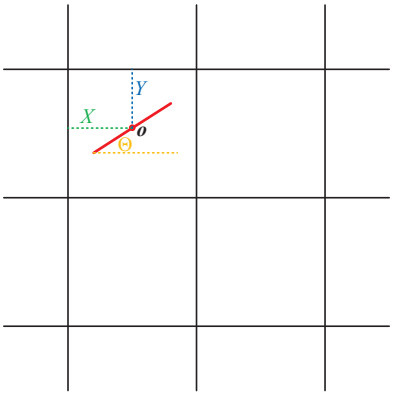

Figure 4: Buffon's needle problem on square grid.

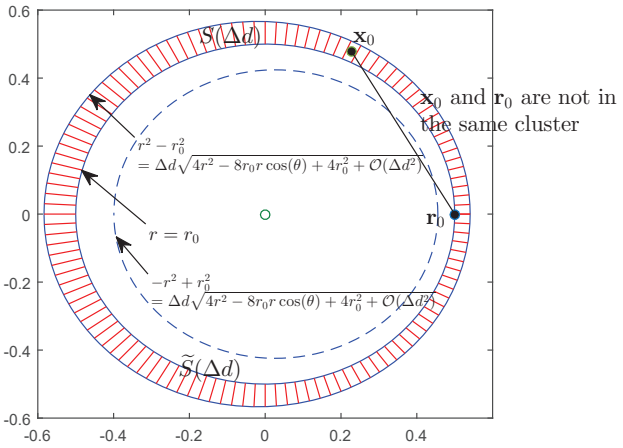

Figure 5: The regions of $S(\Delta d)$ and $\widetilde{S}(\Delta d)$.

Let $\mathbf{x}_0 = (x_0, y_0)$ denote the location of some other BS. Let $\mathcal{T}(\mathbf{r}_0, \mathbf{x}_0)$ denote the trace satisfying the following condition:

$$\mathcal{T}(\mathbf{r}_0, \mathbf{x}_0) = \left\{(x, y) \middle| y_0\left(y - \frac{y_0}{2}\right) = -(x_0 - r_0)\left(x - \frac{x_0 + r_0}{2}\right)\right\}, \tag{49}$$

which is the perpendicular bisector of the line segment with end points $\mathbf{r}_0$ and $\mathbf{x}_0$. The distance from $\mathbf{0}$ to $\mathcal{T}(\mathbf{r}_0, \mathbf{x}_0)$ is

$$d(\mathbf{x}_0, \mathbf{r}_0) = \frac{\left|\frac{y_0^2}{2} - \frac{(r_0 - x_0)(r_0 + x_0)}{2}\right|}{\sqrt{(r_0 - x_0)^2 + y_0^2}}. \tag{50}$$

A necessary condition[4] of $\mathbf{0} \in \mathbf{T}_0^{(2)}(\Delta d)$ is $d(\mathbf{x}_0, \mathbf{r}_0) < \Delta d$, or equivalently, $\mathbf{x}_0 \in \widetilde{S}(\Delta d)$, where

$$\widetilde{S}(\Delta d) = \left\{(x_0, y_0) \middle| \frac{\left|\frac{y_0^2}{2} - \frac{(r_0 - x_0)(r_0 + x_0)}{2}\right|}{\sqrt{(r_0 - x_0)^2 + y_0^2}} < \Delta d\right\}. \tag{51}$$

[4] $\mathbf{0} \in \mathbf{T}^{(2)}(\Delta d)$ iff $d(\mathbf{x}_0, \mathbf{r}_0) < \Delta d$. If we further require $\mathbf{0} \in \mathbf{T}_0^{(2)}(\Delta d)$, the BSs at $\mathbf{x}_0$ and $\mathbf{r}_0$ must belong to two different clusters.

After converting (x_0, y_0) into polar coordinate (r, θ),

$$\widetilde{S}(\Delta d) = \left\{(r, \theta) \middle| |r^2 - r_0^2| < 2\Delta d\sqrt{r_0^2 + r^2 - 2r_0 r\cos\theta + O(\Delta d^2)}\right\}. \tag{52}$$

Note that there are no other BSs located inside $\mathcal{B}(\mathbf{0}, r_0)$. Let $S(\Delta d) = \widetilde{S}(\Delta d) \bigcap \overline{\mathcal{B}(\mathbf{0}, r_0)}$. We have

$$S(\Delta d) = \left\{(r, \theta) \middle| r \geq r_0 \text{ and } \left|r^2 - r_0^2\right| < \Delta d \cdot \sqrt{4r^2 - 8r_0 r\cos(\theta) + 4r_0^2 + O(\Delta d^2)}\right\}. \tag{53}$$

$S(\Delta d)$ corresponds to a "ring" region (shaded area) shown in Fig. 5. The area of $S(\Delta d)$ is

$$\begin{aligned}|S(\Delta d)| =& \int_0^{2\pi}\int_{r_0}^{\sqrt{r_0^2 + 2\Delta d r_0\sqrt{2 - 2\cos(\theta)} + O(\Delta d^2)}} r\mathrm{d}r\mathrm{d}\theta \\ =& 2\Delta d r_0\int_0^{\pi}\sqrt{2 - 2\cos(\theta)}\mathrm{d}\theta + O(\Delta d^2).\end{aligned} \tag{54}$$

Given the reference user and BS, all other BSs are denoted as Φ', which is the reduced Palm point process. Φ' is a PPP with intensity 0 in $\mathcal{B}(\mathbf{0}, r_0)$ and intensity λ in $\overline{\mathcal{B}(\mathbf{0}, r_0)}$. In this situation, $\mathbf{0} \in \mathbf{T}_0^{(2)}(\Delta d)$ if and only if there is at least one BS of Φ' in $S(\Delta d)$ and the BS is not in the same cluster as the reference BS (i.e., the two BSs are in two clusters).

We aim to derive the probability of $\mathbf{0} \in \mathbf{T}_0^{(2)}(\Delta d)$ given the reference BS. In the rest of this proof, for presentation convenience, let E_0 denote the event that the reference BS is located at $\mathbf{r}_0 = (r_0, 0)$; E_1 denote the event that there is exactly one point of Φ' in $S(\Delta d)$; E_2 denote the event that there are more than one points of Φ' in $S(\Delta d)$; and E denote the event that $\mathbf{0} \in \mathbf{T}_0^{(2)}(\Delta d)$. Then we have:

- **(a)** $\mathbb{P}(\mathrm{E}_2|\mathrm{E}_0) = O(\Delta d^2)$.
- **(b)** $\mathbb{P}(\mathrm{E}_1|\mathrm{E}_0) = \lambda|S(\Delta d)| + O(\Delta d^2)$.
- **(c)** Given E_0 and E_1, let $\mathbf{Z}$ denote the location of the point of Φ' in $S(\Delta d)$, then $\mathbf{Z}$ is uniformly distributed in $S(\Delta d)$. Let $\mathrm{pdf}_{\mathbf{Z}|\mathrm{E}_0,\mathrm{E}_1}(\cdot)$ denote the pdf of $\mathbf{Z}$ in this situation.
- **(d)** Given E_0 and E_1, and the location of $\mathbf{Z} = \mathbf{z}$, $\mathbf{0}$ is in $\mathbf{T}_0^{(2)}(\Delta d)$ if and only if the two BSs at $\mathbf{r}_0$ and $\mathbf{z}$ are in different BS clusters (i.e., two different squares). The probability that $\mathbf{r}_0$ and $\mathbf{z}$ are in different BS clusters (denoted by $\mathbb{P}(\mathrm{E}|\mathbf{Z} = \mathbf{z}, \mathrm{E}_1, \mathrm{E}_0)$) depends on the distance between them $|\mathbf{z} - \mathbf{r}_0|$ and the edge length a, which is computed as $P(a, |\mathbf{z} - \mathbf{r}_0|)$ according to Lemma 4.1. (This is a key step to address the challenge in analysis that the two closest BSs do not belong to the same cluster when a handoff occurs.)

Therefore, we have

$$\mathbb{P}(\mathrm{E}|\mathrm{E}_0) \tag{55}$$

$$= \mathbb{P}(\mathrm{E}|\mathrm{E}_1, \mathrm{E}_0)\,\mathbb{P}(\mathrm{E}_1|\mathrm{E}_0) + \mathbb{P}(\mathrm{E}|\mathrm{E}_2, \mathrm{E}_0)\,\mathbb{P}(\mathrm{E}_2|\mathrm{E}_0) \tag{56}$$

$$= \mathbb{P}(\mathrm{E}|\mathrm{E}_1, \mathrm{E}_0)\,\mathbb{P}(\mathrm{E}_1|\mathrm{E}_0) + O(\Delta d^2) \tag{57}$$

$$= \int_{S(\Delta d)} \mathbb{P}(\mathrm{E}|\mathbf{Z} = \mathbf{z}, \mathrm{E}_1, \mathrm{E}_0)\mathrm{pdf}_{\mathbf{Z}|\mathrm{E}_0,\mathrm{E}_1}(\mathbf{z})\,\mathbb{P}(\mathrm{E}_1|\mathrm{E}_0)\,\mathrm{d}\mathbf{z} + O(\Delta d^2) \tag{58}$$

$$r = \int_{S(\Delta d)} P(a, |\mathbf{z} - \mathbf{r}_0|) \frac{1}{|S(\Delta d)|} \left(\lambda |S(\Delta d)| + O(\Delta d^2) \right) \mathrm{d}\mathbf{z} + O(\Delta d^2) \tag{59}$$

$$= \lambda \int_{S(\Delta d)} P(a, |\mathbf{z} - \mathbf{r}_0|) \mathrm{d}\mathbf{z} + O(\Delta d^2) \tag{60}$$

$$= \lambda \int_0^{2\pi} \int_{r_0}^{\sqrt{r_0^2 + 2\Delta d r_0 \sqrt{2 - 2\cos(\theta)} + O(\Delta d^2)}} \left(P(a, r_0 \sqrt{2 - 2\cos(\theta)}) + O(\Delta d) \right) r \mathrm{d}r \mathrm{d}\theta + O(\Delta d^2) \tag{61}$$

$$= 2\Delta d r_0 \lambda \int_0^{\pi} \sqrt{2 - 2\cos(\theta)} P(a, r_0 \sqrt{2 - 2\cos(\theta)}) \mathrm{d}\theta + O(\Delta d^2). \tag{62}$$

where (57) is due to statement (a); (58) is due to the law of total probability; (59) is due to statements (b), (c), and (d); and (61) is due to a conversion form Cartesian coordinate to polar coordinate. Finally, (62) completes the proof. □

REFERENCES

[1] 3GPP-TR-36.819. 2013. Coordinated multi-point operation for LTE physical layer aspects. (Sep. 2013).

[2] S. Akoum and R. W. Heath. 2013. Interference Coordination: Random Clustering and Adaptive Limited Feedback. *IEEE Trans. on Signal Processing* 61, 7 (Apr. 2013), 1822–1834.

[3] A.S. Anpalagan and I. Katzela. 1999. Overlaid Cellular System Design, with Cell Selection Criteria for Mobile Wireless Users. In *Proc. of IEEE Canadian Conference on Electrical and Computer Engineering*. Edmonton, Canada.

[4] F. Ashtiani, J.A. Salehi, and M.R. Aref. 2003. Mobility Modeling and Analytical Solution for Spatial Traffic Distribution in Wireless Multimedia Networks. *IEEE Journal on Selected Areas in Communications* 21, 10 (Dec. 2003), 1699 – 1709.

[5] F. Baccelli and B. Blaszczyszyn. 2009. Stochastic Geometry and Wireless Networks, Volume 1: Theory. *Foundations and Trends in Networking* 3, 3-4 (2009), 249 – 449.

[6] F. Baccelli and B. Blaszczyszyn. 2009. Stochastic Geometry and Wireless Networks, Volume 2: Applications. *Foundations and Trends in Networking* 4, 1-2 (2009), 1–312.

[7] F. Baccelli and A. Giovanidis. 2015. A Stochastic Geometry Framework for Analyzing Pairwise-Cooperative Cellular Networks. *IEEE Trans. on Wireless Communications* 14, 2 (Feb. 2015), 794–808.

[8] Wei Bao and Ben Liang. 2013. Insensitivity of User Distribution in Multicell Networks under General Mobility and Session Patterns. *IEEE Trans. on Wireless Communications* 12, 12 (Dec. 2013), 6244–6254.

[9] Wei Bao and Ben Liang. 2015. Handoff rate analysis in heterogeneous wireless networks with Poisson and Poisson cluster patterns. In *Proc. of ACM MobiHoc*. Hangzhou, China.

[10] Wei Bao and Ben Liang. 2015. Stochastic geometric analysis of user mobility in heterogeneous wireless networks. *IEEE Journal on Selected Areas in Communications* 33, 10 (Oct. 2015), 2212–2225.

[11] Wei Bao and Ben Liang. 2016. Stochastic geometric analysis of handoffs in user-centric cooperative wireless networks. In *Proc. of IEEE INFOCOM*. San Francisco.

[12] Y.C. Chen, J. Kurose, and D Towsley. 2012. A Mixed Queueing Network Model of Mobility in a Campus Wireless Network. In *Proc. of IEEE INFOCOM*. Orlando, FL.

[13] Wang Chi Cheung, T. Q. S. Quek, and M. Kountouris. 2012. Throughput Optimization, Spectrum Allocation, and Access Control in Two-Tier Femtocell Networks. *IEEE Journal on Selected Areas in Communications* 30, 3 (Apr. 2012), 561–574.

[14] H.S Dhillon, R.K. Ganti, F. Baccelli, and J. G. Andrews. 2012. Modeling and Analysis of K-Tier Downlink Heterogeneous Cellular Networks. *IEEE Journal on Selected Areas in Communications* 30, 3 (Apr. 2012), 550–560.

[15] A. Farbod and B. Liang. 2009. Structured admission control policies in heterogeneous wireless networks with mesh underlay. In *Proc. of IEEE INFOCOM*. Rio de Janeiro, Brazil.

[16] Herbert Federer. 1969. *Geometric Measure Theory*. Springer.

[17] Anastasios Giovanidis, Luis David Alvarez Corrales, and Laurent Decreusefond. 2015. Analyzing Interference from Static Cellular Cooperation using the Nearest Neighbour Model. In *Proc. of IEEE Modeling and Optimization in Mobile, Ad Hoc, and Wireless Networks (WiOpt)*. Mumbai, India.

[18] A. Hasib and A.O. Fapojuwo. 2008. Mobility model for heterogeneous wireless networks and its application in common radio resource management. *IET Communications* 2, 9 (Oct. 2008), 1186–1195.

[19] Yateng Hong, Xiaodong Xu, Mingliang Tao, Jingya Li, and Tommy Svensson. 2015. Cross-tier handover analyses in small cell networks: A stochastic geometry approach. In *IEEE International Conference on Communications (ICC)*. London, UK.

[20] Kaibin Huang and J.G. Andrews. 2013. An Analytical Framework for Multicell Cooperation via Stochastic Geometry and Large Deviations. *IEEE Trans. on Information Theory* 59, 4 (Apr. 2013), 2501–2516.

[21] Han-Shin Jo, Young Jin Sang, Ping Xia, and J. G. Andrews. 2012. Heterogeneous Cellular Networks with Flexible Cell Association: A Comprehensive Downlink SINR Analysis. *IEEE Trans. on Wireless Communications* 11, 10 (Oct. 2012), 3484–3495.

[22] Namyoon Lee, David Morales-Jimenez, Angel Lozano, and Robert W. Heath. 2015. Spectral Efficiency of Dynamic Coordinated Beamforming: A Stochastic Geometry Approach. *IEEE Transactions on Wireless Communications* 14, 1 (Jan. 2015), 230–241.

[23] Chang Li, Jun Zhang, M. Haenggi, and K.B.. Letaief. 2015. User-Centric Intercell Interference Nulling for Downlink Small Cell Networks. *IEEE Trans. on Communications* 63, 4 (Apr. 2015), 1419–1431.

[24] Xingqin Lin, R.K. Ganti, P.J. Fleming, and J.G. Andrews. 2013. Towards Understanding the Fundamentals of Mobility in Cellular Networks. *IEEE Trans. on Wireless Communications* 12, 4 (Apr. 2013), 1686–1698.

[25] Yicheng Lin and Wei Yu. 2014. Downlink Spectral Efficiency of Distributed Antenna Systems Under a Stochastic Model. *IEEE Trans. on Wireless Communications* 13, 12 (Dec. 2014), 6891–6902.

[26] A. M. Mathai. 1999. *An Introduction to Geometrical Probability: Distributional Aspects with Applications* (first ed.). CRC Press.

[27] Weili Nie, Fu-Chun Zheng, Xiaoming Wang, Wenyi Zhang, and Shi Jin. 2016. User-Centric Cross-Tier Base Station Clustering and Cooperation in Heterogeneous Networks: Rate Improvement and Energy Saving. *IEEE Journal on Selected Areas in Communications* 5, 34 (May 2016), 1192–1206.

[28] G. Nigam, P. Minero, and M. Haenggi. 2014. Coordinated Multipoint Joint Transmission in Heterogeneous Networks. *IEEE Trans. on Communications* 62, 11 (Nov. 2014), 4134–4146.

[29] Theodore S. Rappaport. 2002. *Wireless Communications: Principles and Practice* (second ed.). Prentice Hall.

[30] Yuwei Ren, Yingzhe Li, and Can Qi. 2017. Handover Rate Analysis for K-Tier Heterogeneous Cellular Networks With General Path-Loss Exponents. *IEEE Communications Letters* 21, 8 (Aug. 2017), 1863– 1866.

[31] S. Sadr and R.S. Adve. 2015. Handoff Rate and Coverage Analysis in Multi-Tier Heterogeneous Networks. *IEEE Trans. on Wireless Communications* 14, 5 (May 2015), 2626–2638.

[32] N. Shenoy and B. Hartpence. 2004. A mobility model for cost analysis in integrated cellular/WLANs. In *Proc. of International Conference on Computer Communications and Networks*. Chicago, IL.

[33] Sarabjot Singh and Jeffrey G. Andrews. 2014. Joint Resource Partitioning and Offloading in Heterogeneous Cellular Networks. *IEEE Trans. on Wireless Communications* 13, 2 (Feb. 2014), 888 – 901.

[34] D. Stoyan, W. Kendall, and J. Mecke. 1995. *Stochastic Geometry and Its Applications* (second ed.). Wiley.

[35] R. Tanbourgi, S. Singh, J.G. Andrews, and F.K. Jondral. 2014. A Tractable Model for Noncoherent Joint-Transmission Base Station Cooperation. *IEEE Trans. on Wireless Communications* 13, 9 (Jul. 2014), 4959–4973.

[36] Sanford Weisberg. 2005. *Applied Linear Regression* (third ed.). Wiley.

[37] Ping Xia, Chun-Hung Liu, and J.G. Andrews. 2013. Downlink Coordinated Multi-Point with Overhead Modeling in Heterogeneous Cellular Networks. *IEEE Trans. on Wireless Communications* 12, 8 (Aug. 2013), 4025–4037.